ADVANCED FUNCTIONAL MATERIALS
www.afm-journal.de

Functional Free-Standing Graphene Honeycomb Films

*Shengyan Yin, Yulia Goldovsky, Moshe Herzberg, Lei Liu, Hang Sun, Yanyan Zhang, Fanben Meng, Xuebo Cao, Darren D. Sun, Hongyu Chen, Ariel Kushmaro, and Xiaodong Chen**

Fabricating free-standing, three-dimensional (3D) ordered porous graphene structure can service a wide range of functional materials such as environmentally friendly materials for antibacterial medical applications and efficient solar harvesting devices. A scalable solution processable strategy is developed to create such free-standing hierarchical porous structures composed of functionalized graphene sheets via an "on water spreading" method. The free-standing film shows a large area uniform honeycomb structure and can be transferred onto any substrate of interest. The graphene-based free-standing honeycomb films exhibit superior broad spectrum antibacterial activity as confirmed using green fluorescent protein labeled *Pseudomonas aeruginosa* PAO1 and *Escherichia coli* as model pathogens. Functional nanoparticles such as titanium dioxide (TiO_2) nanoparticles can be easily introduced into conductive graphene-based scaffolds by premixing. The formed composite honeycomb film electrode shows a fast, stable, and completely reversible photocurrent response accompanying each switch-on and switch-off event. The graphene-based honeycomb scaffold enhances the light-harvesting efficiency and improves the photoelectric conversion behavior; the photocurrent of the composite film is about two times as high as that of the pure TiO_2 film electrode. Such composite porous films combining remarkably good electrochemical performance of graphene, a large electrode/electrolyte contact area, and excellent stability during the photo-conversion process hold promise for further applications in water treatment and solar energy conversion.

1. Introduction

Assembly of graphene nanosheets into macroscopic structures (e.g., layered films and porous scaffolds) have garnered increasing attention, since it is an important step in exploring the advanced properties of individual graphene sheets for macroscopic applications, such as energy storage and converison,[1] catalysis,[2] chemical filtration,[3] sensing,[4] and selective organic absorption.[5] Although different methods, such as filtration,[6] molecular templates,[7] Langmuir–Blodgett assembly,[8] layer-by-layer assembly,[9] and direct chemical vapor deposition on selected substrates,[10] have been used to assemble graphene nanosheets into ordered microstructure films, rationally designed macroscopic architectures that offer a scope to probe additional fundamental scientific opportunities,[11] such as the collective electronic and mechanical properties,[12] are still needed. Fabricating and assembling known materials into hitherto unchartered materials realm offers exciting possibilities to shape and mould materials of specific design and

Dr. S. Yin, Y. Zhang, F. Meng, Dr. X. Cao,
Dr. A. Kushmaro, Prof. X. Chen
School of Materials Science and Engineering
Nanyang Technological University
50 Nanyang Avenue
Singapore 639798, Singapore
E-mail: chenxd@ntu.edu.sg
Y.Go ldovsky
Unit of Environmental Engineering
Ben-Gurion University of the Negev
P. O. Box 653, Beer-Sheva 84105, Israel
Dr. M. Herzberg
Ben Gurion University of the Negev
Zuckerberg Institute for Water Research
Sede Boqer Campus
Midreshet Ben Gurion 84990, Israel
L. Liu, Prof. D. D. Sun
School of Civil and Environmental Engineering
Nanyang Technological University
50 Nanyang Avenue, Singapore 639798, Singapore
Dr. H. Sun, Prof. H. Chen
Division of Chemistry & Biological Chemistry
School of Physical and Mathematical Sciences
Nanyang Technological University
21 Nanyang Link, Singapore 637371, Singapore
Dr. A. Kushmaro
Avram and Stella Goldstein-Goren
Department of Biotechnology
Engineering and National Institute for
Biotechnology in the Negev
Ben-Gurion University of the Negev
Beer-Sheva 84105, Israel

DOI:10. 1002/adfm.201203491

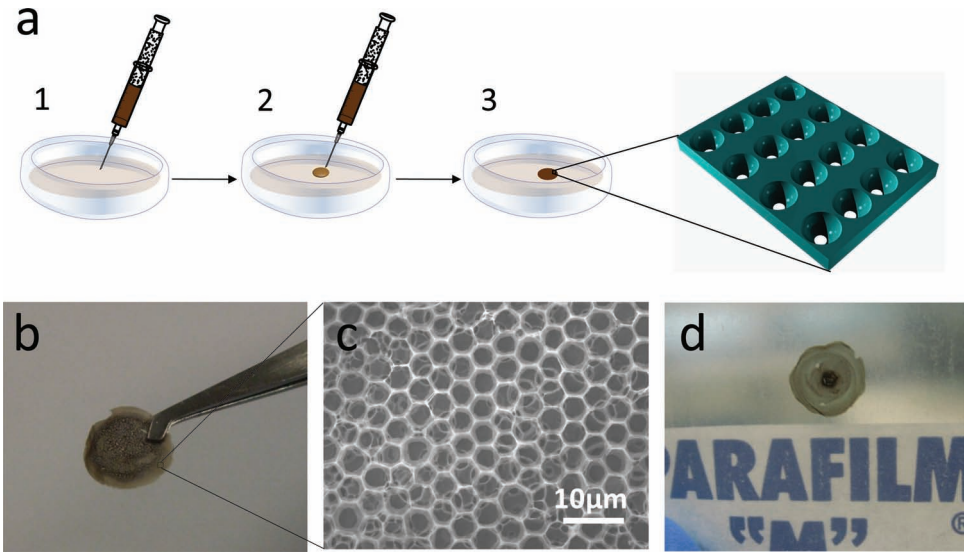

Figure 1. a) Schematic drawing of the preparation of a free-standing honeycomb film using the GO/DODA complex. b) Photograph and c) SEM image of the free-standing honeycomb film. d) Photograph of the self-supporting honeycomb film transferring onto Parafilm.

utility. We undertook the challenge of developing a facile synthesis technique to generate self-supporting, three-dimensinal (3D) ordered porous graphene films. Specifically, porous films are known to exhibit enhanced performance in sensors, optical devices, energy storage, and chemical separation.[5,13] Ordered porous structures would significantly improve the photoelectric effect of thin-film devices, for example, when graphene is used as the electron acceptor in dye-sensitized solar cells and polymer solar cells.[14] Going a step further, the free-standing hierarchical porous graphene film may also serve as reinforcement to enhance mechanical, thermal, or electrical properties in composite materials.[15] Taken together, free-standing and hierarchical porous architecture would enable graphene itself to serve as both the substrate and the active material, which can maximize device optimization.

Here, we introduce a low-cost facile strategy to create such free-standing hierarchical porous structures composed of graphene sheets via an "on water spreading" method[16] based on our previous experience in fabricating graphene sheets using the breath figure method.[13a] The resultant films are conductive and exhibit robust chemical stability in addition to superior antibacterial properties and improved photoresponse when combined with titanium dioxide (TiO_2) nanoparticles. The rational design and engineering of the nanocomposite fabrication process avoids the risk of inhaling nanoparticles, poor flow and handling as well as metering and control. The advantages and potential applications are striking, such as environmentally friendly materials for antibacterial water treatment and medical applications and more efficient solar harvesting devices.

2. Results and Discussion

2.1. Preparation of Free-Standing Graphene Honeycomb Films

Experimentally, the complex of graphene oxide (GO) and dimethyldioctadecylammonium (DODA) is prepared by the phase-transfer method in line with our previous work,[13a] which has been described in detail in the Experimental Section. The as-prepared complex is not soluble in water but readily dissolves in organic media such as chloroform, dichloromethane, benzene, and so forth, resulting in transparent solutions. Hence, it can be extrapolated that the hydrophilic surface of GO has been successfully modified by the hydrophobic alkyl chains of surfactants, and that the surfactant molecule can prevent the collapse and aggregation of adjacent graphene layers when the GO is reduced to rGO. The GO/DODA chloroform solution (1 mg/mL) is then cast drop-by-drop onto the water surface (temperature 25 °C) to form a thin film as shown in **Figure 1**a. After the complete evaporation of chloroform within 1–2 min under the moist environment,[16] the brown thin film remains floating on the water surface. The as-formed film is flexible and robust, and can be lifted by a pair of tweezers to obtain the self-supporting film (Figure 1b). These films shine in bright iridescent colors when viewed with reflected light, indicating a periodic variation in the refractive index throughout the thickness of the film. Figure 1c shows a representative SEM image of the free-standing film prepared from 1 mg/mL of GO/DODA complex in chloroform. The top view of the SEM image (Figure 1c) reveals the ordered hexagonal structure across a large area with uniform pores with an average diameter of about 2.8 μm and an interval of about 0.8 μm between adjacent holes. Significantly, the variation in humidity did not affect the porous structure of the film once formed. The film could further be transferred onto various substrates, including glass, silicon substrate, organic polyethylene terephthalate (PET) film, and even hydrophobic Parafilm (Figure 1d), on which traditionally, a honeycomb film cannot be prepared by breath figure method since the casting chloroform solution destroys the organic substrates. It is noted that the resulting films were no longer soluble in any organic solvent or water once reduced.

Table 1. IMARIS analysis of specific biovolume ($\mu m^3/\mu m^2$) in the biofilm layer after 24 and 48 h incubation.

		Graphene honeycomb film	Graphite
24 h	Dead	2.45 ± 0.89	0.64 ±0. 05
	Live	0.97 ± 1.82	5.65 ±5. 90
	EPS	0.40 ± 0.15	3.20 ±1. 42
48 h	Dead	4.21 ± 0.50	5.38 ±3. 05
	Live	3.48 ± 0.06	5.55 ±1. 98
	EPS	0.85 ± 0.18	7.13 ±3. 15

2.2. The Antibacterial Activity of Free-Standing Honeycomb Films

Since the free-standing graphene honeycomb film combines flexibility and mechanical stiffness, it could potentially be used as varied as water treatment or as scaffolds for cell growth,[17] a common requirement for both being the antibacterial property. Then, the first requirement for such potential application should be antibacterial. We transferred the free-standing honeycomb film onto glass slides or glass fiber membrane, and reduced it with hydrazine monohydrate, which has been described in detail in the Experimental Section. The antibacterial activity of free-standing honeycomb films was tested using green fluorescent protein labeled *Pseudomonas aeruginosa* PAO1 and *E. coli* as model pathogens,[18] and cells grown on graphite as control. Laser scanning confocal microscopy (LSCM) was used to observe the samples in real-time and LSCM images were analyzed using IMARIS-Bitplane software. As indicated by the calculated data in **Table 1**, after 24 h incubation, there were more dead cells and fewer live cells on the graphene honeycomb film than that on the graphite in a specific biovolume ($\mu m^3/\mu m^2$) of the biofilm layer. After 48 h incubation, although there were several dead cells on the graphite, the ratio of the live cells to dead cells was higher than that on the graphene honeycomb film which contained significantly more dead cells. Furthermore, there was a greater amount of extracellular polymeric substance (EPS), indicative of a thriving biofilm on the graphite, consistent with the microscopy images as shown in **Figure 2**. SEM and optical images were in good alignment indicating robust growth of intact cells on the graphite (Figure 2d inset) as against cells with disrupted membranes on the graphene honeycomb film (Figure 2c, inset).

We also use anther model pathogen, *E. coli*,[19] which were sprayed onto the Luria-Bertani growth medium, to study the antibacterial property of the honeycomb film. After 24 h inoculation, we could not find any obvious bacterial cell growth on the honeycomb films as shown in **Figure 3**a. The SEM images also show that the number of *E. coli* cells on the commercial glass fiber membrane outnumbered the number of cells on the graphene honeycomb film (Figure 3b,c). It is noted that there is no observable change on the morphology of the films before and after antibacterial experiments. All these illustrate that our graphene-based free-standing honeycomb films have excellent broad spectrum antibacterial activity, which combines the exceptional mechanical strength, electrical conductivity, and biocompatibility of graphene[20] and the increased surface area of honeycomb structure, and thus shows a promising application for a cell growth incubator and biomedical electrochemical sensing analysis.

The commonly used method for the preparation of an antibacterial porous film is through loading antibacterial agents, such as metal ions,[21] silver nanoparticles,[22] quaternary

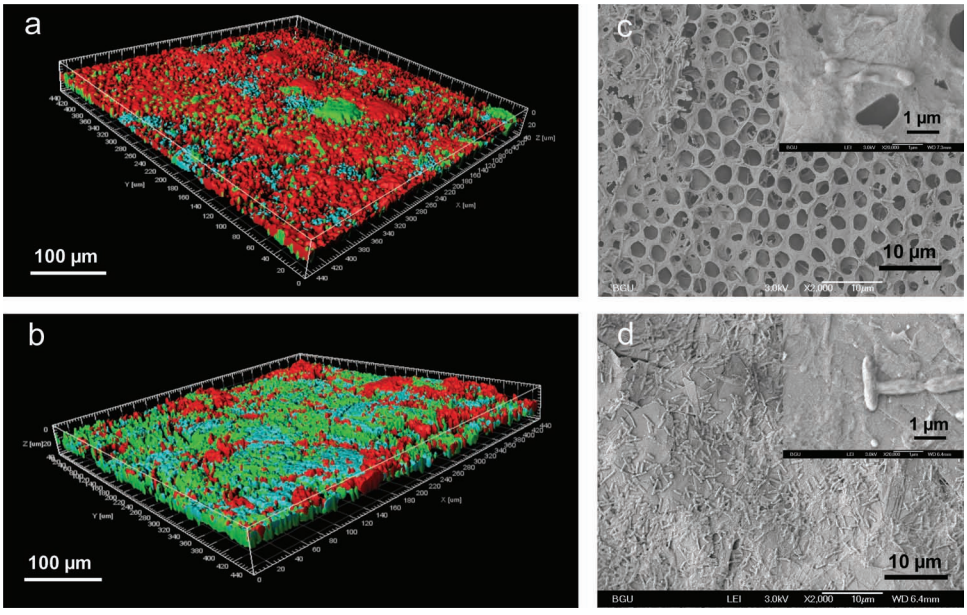

Figure 2. Laser scanning confocal microscopy images of green fluorescent protein labeled *Pseudomonas aeruginosa* PAO1 biofilm on a) graphene honeycomb film and b) graphite surface after 48 h incubation. The biofilm stained with live (green), dead (red) and EPS (blue) kit. SEM images of green fluorescent protein labeled *Pseudomonas aeruginosa* PAO1 biofilm on c) graphene honeycomb film and d) graphite surface after 48 h incubation; insets are the amplified images of *Pseudomonas aeruginosa* PAO1.

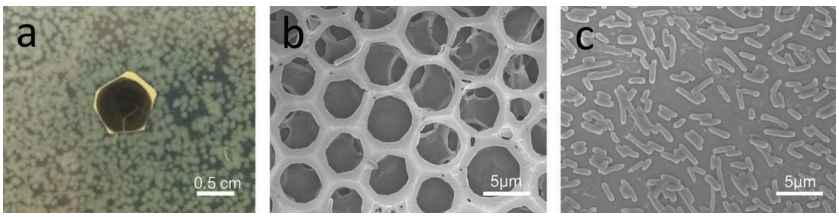

Figure 3. Antibacterial properties of the free-standing honeycomb film. a) Photograph of *E. coli* grown on honeycomb film (after incubation at 37 °C overnight); SEM images of *E. coli* attached to b) honeycomb film and c) glass fiber membranes (after incubation at 37 °C for 24 h).

ammonium compounds,[23] or carbon nanotubes[24] into the films. However, the gradual leaks of the loaded additives may contaminate the surrounding environment while the honeycomb film may reduce the antibacterial activity.[25] Recently, it was reported that the flatten graphene films have antibacterial property.[19] Here, however, we directly use GO/DODA complex to prepare antibacterial porous film, in which both rGO (formed after reduction of GO) and DODA (a kind of quaternary ammonium compound) have antibacterial activity, and thus no additional antibacterial agent is needed. Furthermore, rGO/DODA complex is formed by electrostatic interaction which avoids the possible leaks (DODA is water insoluble), and thus ideal antibacterial honeycomb film could be expected in our system.

2.3. Photoelectrochemical Properties of Composite Free-standing Honeycomb Films

The interest in photovoltaic devices has long been motivated by the need to supplement fossil fuels with clean and renewable energy resources.[14b] Due to its strong oxidizing power, high activity, low cost, high chemical inertness, non-toxicity, and photostability,[26] TiO_2 is widely used in this field. One of the bottlenecks of increasing the conversion efficiency in photovoltaic devices is the transport of photogenerated electrons across the TiO_2 nanoparticle network as it competes with charge recombination. To suppress the recombination and improve the transport of the photogenerated electrons, there are several strategies including (1) doping metal ions or other elements (such as N),[27] (2) preparing a porous structure whose direction is perpendicular to the conducting substrate,[28] and (3) introducing charge carriers to direct photogenerated electrons.[29] Therefore, fabricating a porous structure with the graphene and TiO_2 nanoparticles can simultaneously combine the positive effects of latter two parts, whereby the graphene honeycomb structure acts as the scaffold and creates a 2D conductive support path for charge transport between TiO_2 nanoparticles and offer a solution to suppress the recombination and enhance the photoelectric conversion efficiency.

Here, as a proof-of-concept experiment, free-standing honeycomb composite film with graphene and TiO_2 nanoparticles (P25) was prepared as shown in **Figure 4**a. A droplet of GO/DODA/P25 mixture solution was spread on the surface of water and upon the evaporation of the chloroform solvent, the water vapor condensed on the surface to work as the template. During the chloroform solvent evaporation, the TiO_2 nanoparticles spontaneously assembled into the interfaces of water/chloroform as a result of the Pickering emulsions effect.[30] The top view of the SEM image (Figure 4b) indicates that the obtained free-standing graphene honeycomb composite film exhibits a uniform porous structure and the TiO_2 nanoparticles had little effect on the order and pore size of the free-standing honeycomb structure. The magnified TEM image (Figure 4c) suggests that TiO_2 nanoparticles enriched the walls of the porous structure, leaving the center of the pore was intact. In such a hybrid structure, synergistic effect between TiO_2 and graphene would benefit the electron transport and suppress the recombination.

Subsequently, the N_2H_4 vapor was used to deoxidize the free-standing honeycomb film to the reduced (rGO/DODA/P25) film, while the honeycomb structures remained intact, confirmed by Raman spectra measurements[13a] For the GO/DODA/P25 honeycomb films, there were two prominent peaks at 1570 and 1336 cm^{-1} corresponding to the well documented G and D bands.[9,31] After the reduction, the G and D bands could still be detected, but the values of I_D/I_G increased in comparison to the GO/DODA/P25 film, strongly suggesting that the conversion of GO to rGO in the honeycomb films after exposure to N_2H_4 vapor (Figure 4d). The peaks at 189, 394, 517, and 639 can be assigned as the $[E_g(2)]$, $[B_{1g}(1)]$, $[A_{1g}]$ or $[B_{1g}(2)]$, and $[E_g(3)]$ modes of the anatase phase,[32] respectively, which confirms the successful introduction of TiO_2 nanoparticles to the honeycomb film. Post-reduction, the observable characteristic peaks of TiO_2 suggest that TiO_2 nanoparticles remained stable during the reduction (Figure 4d). Thus, the Raman spectra confirmed the presence and stability of free-standing film mixed with TiO_2 nanoparticles before and after the reduction process. Moreover, the electrical resistivity of the rGO/DODA and the rGO/DODA/P25 honeycomb films was measured to be 8.8 Ωm and 120.1 Ωm (**Figure 5** a). Although the reduced graphene sheets were disordered in their distribution within the frame of the honeycomb films, the edge contacts between the reduced graphene sheets still guaranteed the conductivity of the whole film, which ensured efficient electron transport for electrical devices. The higher resistivity of the rGO/DODA/P25 honeycomb film compared to the rGO/DODA honeycomb film implied that the TiO_2 nanoparticles dispersed well within the graphene sheets, and this further suppressed the recombination and enhanced the photoelectric conversion properties of the composite film.

To further characterize the effect of the antireflection on the graphene honeycomb film, we have conducted standard absolute hemispherical reflectance measurement with an integrating sphere at normal incidence. The reflectance measurement was carried out over a broad wavelength range (200–800 nm) which covers most of the solar spectrum. As shown in Figure 5b, the diffuse reflectivity measurements indicate that up to 16% of the incident light is reflected on the ITO glass compared to the graphene honeycomb (rGO/DODA) film. Significantly, the rGO/DODA/P25 composite free-standing films can be further reduced to less than 4% reflected light at UV range by introduced the TiO_2 nanoparticles (red curve of Figure 5b). These results show that the composite honeycomb film increase the light absorption. Photocurrent measurements were carried out

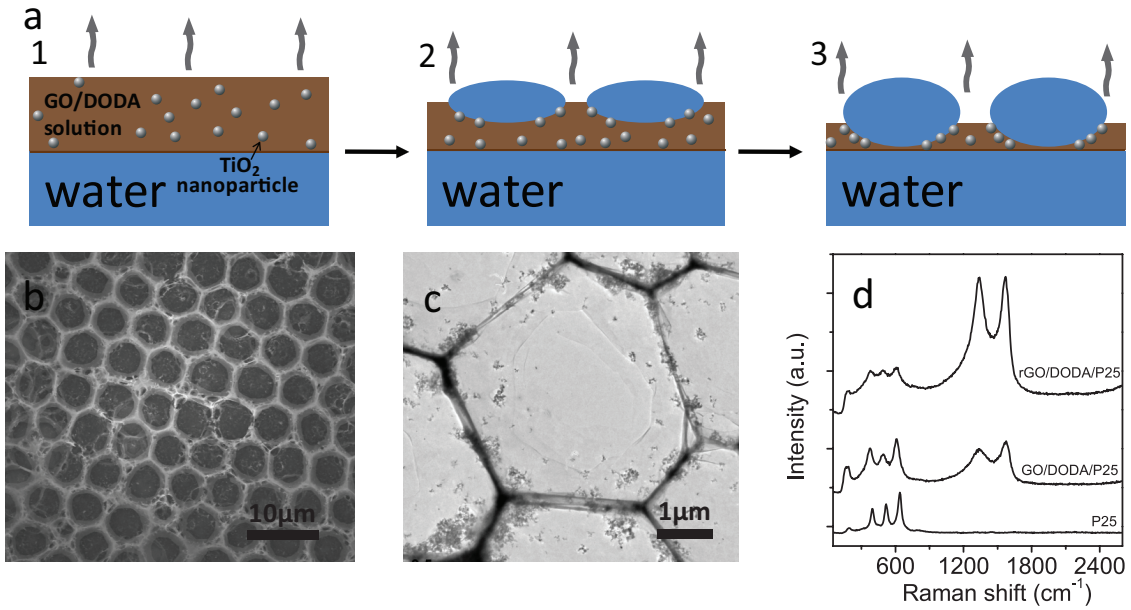

Figure 4. a) Schematic representation of the formation of the composite free-standing honeycomb film with the TiO_2 nanoparticles (P25): (1) spreading GO/DODA/P25 chloroform on the surface of water; (2) condensing water droplet on the chloroform surface and evaporating the chloroform simultaneously; and (3) spontaneously assembling TiO_2 nanoparticles at the interfaces of water/chloroform due to the Pickering emulsion effect. b) SEM image of GO/DODA/P25 free-standing honeycomb film. c) Magnified TEM image of GO/DODA/P25 free-standing honeycomb film. d) Raman spectra of the free-standing honeycomb films of rGO/DODA/P25, GO/DODA/P25, and TiO_2 nanoparticles (from top to bottom) under the 488 nm laser excitation.

on the as-prepared rGO/DODA/P25 composite free-standing films by transferring the films onto the ITO glass to act as electrodes. As shown in the typical *I–V* curves of the rGO/DODA/P25 composite films device, with and without the irradiation of a continuous light in Figure 5c, the current drastically increased when light was irradiated. Photocurrent properties of two honeycomb films with and without TiO_2 nanoparticles were also compared with the pure TiO_2 film (same amount of TiO_2) as the control. The potential of the working electrode was set at 0 V (vs Ag/AgCl). A fast, stable, and completely reversible photocurrent response was observed accompanied each switch-on and the switch-off event in the rGO/DODA/P25 and P25 film electrodes (Figure 5d). The photocurrent of the as-prepared rGO/DODA/P25 composite free-standing film electrode was about two times as high as that of the TiO_2 film electrode. The improved photocurrent performance should be ascribed to the synergistic effects of the following factors. First of all, the increased photoresponse could be ascribed to the strong anchoring of TiO_2 nanoparticles in rGO, so that the photoinduced electrons were captured by the graphene easily, in other word, the separation efficiency of photoinduced electrons and holes was improved through the electronic interaction between graphene and TiO_2.[14d] Additionally, graphene holds promise as a transparent conductor because of its unique electronic structure[33] bearing little effect on the light irradiating on the TiO_2 nanoparticles which are wrapped by graphene sheets or under several graphene layers. Finally, the porous structure of the electrode may reduce reflection of light,[14a] which boosts the light capture inside the film and enhances the light-harvesting efficiency, and thus significantly improving the photoelectric conversion behavior. Hence, fabrication of a porous structure with graphene and nanoparticles offer an unparalleled method to enhance the photoelectric conversion properties.

3. Conclusions

In summary, we developed a facile strategy to fabricate a free-standing graphene honeycomb composite film via "on water spreading" method. The free-standing film shows a large area uniform honeycomb structure and can be transferred onto any substrates of interest. The process to form such structure is simple, solution processable, and environment friendly. Furthermore, the obtained graphene-based free-standing honeycomb films show excellent broad spectrum antibacterial activity. Finally, it is easy to introduce functional nanoparticles into the free-standing graphene honeycomb film by premixing to form functional hybrid film. The honeycomb structures provide enhanced light harvesting properties, which is beneficial for increasing the efficiency of light conversion. Therefore, such composite porous film combining remarkably good electrochemical performance of graphene, the large electrode/electrolyte contact area, and excellent stability during the photoconversion process holds promise for further applications in water treatment and solar energy conversion.

4. Experimental Section

Preparation of the Surfactant Encapsulated Graphene Oxide (GO): GO was prepared from natural graphite powder (Sigma, 45 μm) via

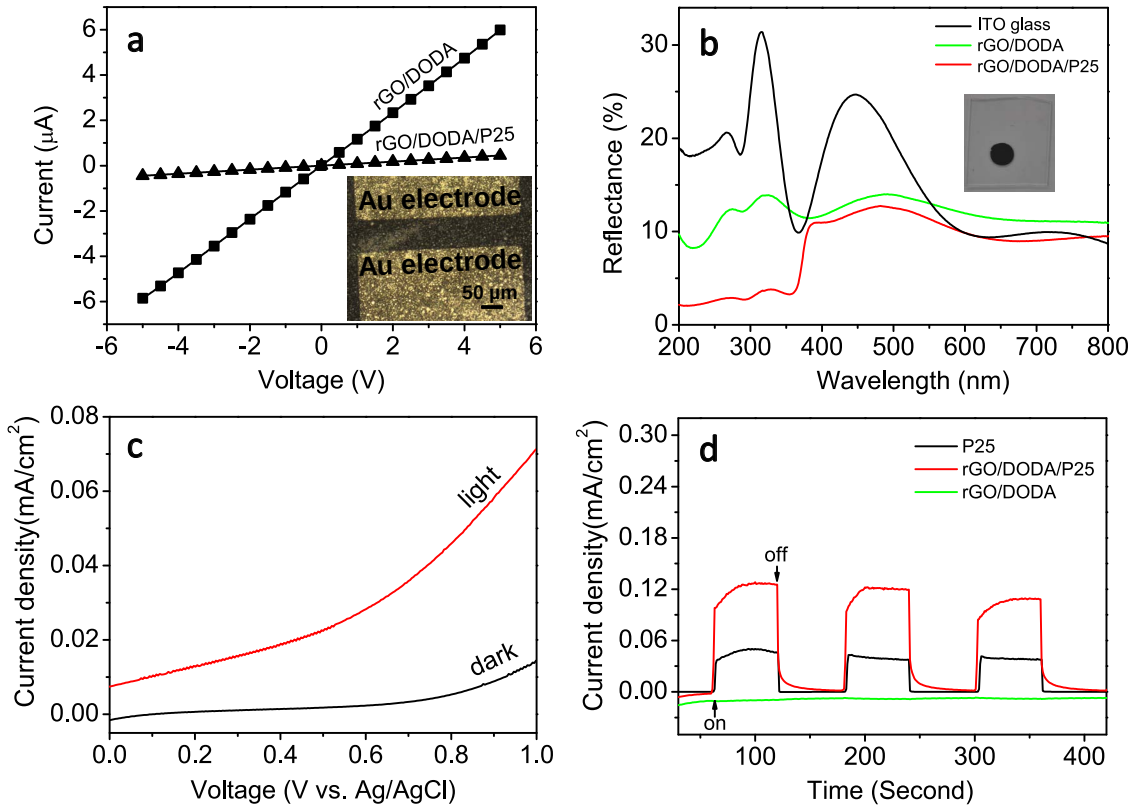

Figure 5. a) Conductivity measurement of the free-standing honeycomb film (inset: the microscopy image of the device for conductivity measurement); b) Reflectance spectra of ITO glass (black), rGO/DODA (green), and rGO/DODA/P25 (red) respectively (inset: the photograph of the rGO/DODA/P25 film on the ITO glass); c) Typical *I–V* characteristic of the rGO/DODA/P25 free-standing honeycomb film in the absence and presence of irradiation; d) Current versus time under chopped irradiation of rGO/DODA/P25 (red), rGO/DODA (green), and P25 (black), at a bias voltage of 0 V (vs Ag/AgCl).

a modified Hummers method.[34] To ensure the formation of a single layer of GO, the GO solution was subjected to 30 min of centrifugation at 14 000 rpm. The clear top solution was taken, and its pH adjusted to approximately 9 with 1 mol/L NaOH. Subsequently, chloroform solution containing 1 mg/mL dimethyldioctadecylammonium (DODA) was selected to titrate the GO water solution. When the color of water solution changed to light brown, DODA chloroform solution was no longer added. The organic phase was then separated to obtain GO/DODA complex in the chloroform solution.

Preparation of the Free-Standing Honeycomb Films: We used the on-water spreading method to build the honeycomb films.[16] Typically, the free-standing honeycomb thin films were prepared by direct casting 50 μL of GO/DODA complex chloroform solution (1 mg/mL) onto the water surface. After the chloroform vaporized completely, another 50 μL of GO/DODA complex chloroform solution was added. The humid conditions were achieved by water vapor itself (25 °C). The brown thin films covering an area of ca. 1.5 cm^2 were left behind after the complete evaporation of the solvent within 1–2 min. The GO/DODA honeycomb films floating on the water surface were transferred to a substrate such as an ITO glass or used as free-standing films. To reduce the free-standing honeycomb films, we autoclaved the films, added 10 μL hydrazine monohydrate into the reactor, and heated the reactor at 90 °C for 16 h. The same protocol was followed to prepare the free-standing film composite with TiO_2 nanoparticles (P25). The GO/DODA solution containing TiO_2 nanoparticles was prepared by adding 10 μL 10 mg/mL TiO_2 nanoparticles ethanol solution into 1 mL of 1 mol/L GO/DODA chloroform solution.

Antibacterial Activity Test: The green fluorescent protein labeled *Pseudomonas aeruginosa* PAO1 was grown in Luria-Bertani nutrient solution by incubating in a shaker-incubator at 150 rpm and 30 °C (ZHWY-1102C, ZHWY, China). A fresh colony was harvested and grown in Luria-Bertani broth medium at 30 °C for 3 h(OD_{600} ≈ 0.6) to serve as the inoculum for the antibacterial experiments. Samples were stained with concanavalin A (Con A), SYTO 9 and propidium iodide (PI) (Invitrogen, Eugene, Oregon, USA) for probing EPS, live and dead cells, respectively. The laser scanning confocal microscopy (LSCM) scale images were analyzed using IMARIS-Bitplane software and the specific biovolumes ($\mu m^3/\mu m^2$) and 3D reconstruction of the biofilms were also carried out with IMARIS-Bitplane software. The morphological changes of *Pseudomonas aeruginosa* PAO1 cells on honeycomb films were investigated by scanning electron microscopy (SEM). After 48 h inoculation, the membrane samples on agar plates were quickly fixed with 2.5% glutaraldehyde. Then, the samples were dehydrated with sequential treatment with 25, 50, 75, 95, and 100% ethanol for 10 min. The samples were freeze dried at −50 °C before SEM testing. *E. coli* K12 ER2925 (New England Biolab) was cultivated in Luria-Bertani nutrient solution at 37 °C for 18 h to get the exponential growth phase. The cells were harvested by centrifugation at 6000 rpm with phosphate buffer solution (PBS, pH 7.2), and washed with saline solution (0.9% NaCl) to remove residual macromolecules. The cells were diluted to 10^4–10^5 colony forming units (cfu/mL), and sprayed onto Luria-Bertani culture medium plates. After 1 h at 37 °C, the honeycomb films (using glass fiber as a support layer, ADVAVTEC, GC-50, 0.45 μm) were gently placed on the top of the inoculated agar plates for the cells to interact with the materials. These plates were incubated at 37 °C for 24 h. Control experiment with commercial glass fiber membranes were conducted at the same condition. SEM samples were prepared using the same method as mentioned above. All glassware and solutions used in the experiments were autoclaved at 121 °C for 20 min to ensure sterility.

Photocurrent Measurements: The free-standing honeycomb films were transferred on the 2 cm × 3 cm ITO glass. For the pure TiO_2 films as the control experiment, in order to have the same amount of TiO_2 and similar morphology, they were prepared from GO/DODA/P25 honeycomb films by thermal removing graphene and organic component. Photocurrent measurements were performed in a three-electrode cell that was connected to a CHI 660D electrochemical station (CH Instruments), in which the free-standing honeycomb films acted as working electrode, Ag/AgCl as reference electrode (3.0 M KCl) and a Pt mesh as counter electrode. The electrolyte was 0.5 M Na_2SO_4 solution, and was purged with nitrogen for 1 h. A high-pressure Xe lamp was used as light source to simulate solar light. The light intensity was 100 mW/cm^2 and the area of the sample exposed to light was 1.5 cm^2.

Acknowledgements

This work was supported by the Singapore National Research Foundation (CREATE Programme of Nanomaterials for Energy and Water Management and NRF-RF2009-04).

Received: November 26, 2012
Published online: January 17, 2013

[1] a) S. H. Lee, H. W. Kim, J. O. Hwang, W. J. Lee, J. Kwon, C. W. Bielawski, R. S. Ruoff, S. O. Kim, *Angew. Chem. Int. Ed.* **2010**, *49*, 10084; b) S. Yang, Y. Sun, L. Chen, Y. Hernandez, X. Feng, K. Müllen, *Sci. Rep.* **2012**, *2*, 427; c) L. Dai, D. W. Chang, J.-B. Baek, W. Lu, *Small* **2012**, *8*, 1130; d) J. Liu, X.-W. Liu, *Adv. Mater.* **2012**, *24*, 4097; e) Y. Xu, K. Sheng, C. Li, G. Shi, *ACS Nano* **2010**, *4*, 4324; f) B. Luo, S. Liu, L. Zhi, *Small* **2012**, *8*, 630.

[2] a) G. M. Scheuermann, L. Rumi, P. Steurer, W. Bannwarth, R. Mülhaupt, *J. Am. Chem. Soc.* **2009**, *131*, 8262; b) L. Qu, Y. Liu, J.-B. Baek, L. Dai, *ACS Nano* **2010**, *4*, 1321.

[3] D. Cohen-Tanugi, J. C. Grossman, *Nano Lett.* **2012**, *12*, 3602.

[4] a) F. Schedin, A. K. Geim, S. V. Morozov, E. W. Hill, P. Blake, M. I. Katsnelson, K. S. Novoselov, *Nat. Mater.* **2007**, *6*, 652; b) F. Yavari, Z. Chen, A. V. Thomas, W. Ren, H.-M. Cheng, N. Koratkar, *Sci. Rep.* **2011**, *1*, 166.

[5] Z. Niu, J. Chen, H. H. Hng, J. Ma, X. Chen, *Adv. Mater.* **2012**, *24*, 4144.

[6] D. A. Dikin, S. Stankovich, E. J. Zimney, R. D. Piner, G. H. B. Dommett, G. Evmenenko, S. T. Nguyen, R. S. Ruoff, *Nature* **2007**, *448*, 457.

[7] Z. Wei, D. E. Barlow, P. E. Sheehan, *Nano Lett.* **2008**, *8*, 3141.

[8] L. J. Cote, F. Kim, J. Huang, *J. Am. Chem. Soc.* **2008**, *131*, 1043.

[9] J. Shen, Y. Hu, C. Li, C. Qin, M. Shi, M. Ye, *Langmuir* **2009**, *25*, 6122.

[10] D. Wei, Y. Liu, Y. Wang, H. Zhang, L. Huang, G. Yu, *Nano Lett.* **2009**, *9*, 1752.

[11] S. Yin, Z. Niu, X. Chen, *Small* **2012**, *8*, 2458.

[12] N. A. Kotov, *ACS Nano* **2009**, *3*, 1307.

[13] a) S. Yin, Y. Zhang, J. Kong, C. Zou, C. M. Li, X. Lu, J. Ma, F. Y. C. Boey, X. Chen, *ACS Nano* **2011**, *5*, 3831; b) K. E. Shopsowitz, H. Qi, W. Y. Hamad, M. J. MacLachlan, *Nature* **2010**, *468*, 422; c) R. Vendamme, S.-Y. Onoue, A. Nakao, T. Kunitake, *Nat. Mater.* **2006**, *5*, 494; d) C. Jiang, S. Markutsya, Y. Pikus, V. V. Tsukruk, *Nat. Mater.* **2004**, *3*, 721; e) J. Chen, K. Sheng, P. Luo, C. Li, G. Shi, *Adv. Mater.* **2012**, *24*, 4569.

[14] a) L. Heng, J. Zhai, Y. Zhao, J. Xu, X. Sheng, L. Jiang, *ChemPhysChem* **2006**, *7*, 2520; b) Y.-B. Tang, C.-S. Lee, J. Xu, Z.-T. Liu, Z.-H. Chen, Z. He, Y.-L. Cao, G. Yuan, H. Song, L. Chen, L. Luo, H.-M. Cheng, W.-J. Zhang, I. Bello, S.-T. Lee, *ACS Nano* **2010**, *4*, 3482; c) L. Gomez De Arco, Y. Zhang, C. W. Schlenker, K. Ryu, M. E. Thompson, C. Zhou, *ACS Nano* **2010**, *4*, 2865; d) N. Yang, J. Zhai, D. Wang, Y. Chen, L. Jiang, *ACS Nano* **2010**, *4*, 887.

[15] a) S. Stankovich, D. A. Dikin, G. H. B. Dommett, K. M. Kohlhaas, E. J. Zimney, E. A. Stach, R. D. Piner, S. T. Nguyen, R. S. Ruoff, *Nature* **2006**, *442*, 282; b) G. Eda, M. Chhowalla, *Nano Lett.* **2009**, *9*, 814; c) J. K. Koh, J. Kim, B. Kim, J. H. Kim, E. Kim, *Adv. Mater.* **2011**, *23*, 1641; d) A. Boker, Y. Lin, K. Chiapperini, R. Horowitz, M. Thompson, V. Carreon, T. Xu, C. Abetz, H. Skaff, A. D. Dinsmore, T. Emrick, T. P. Russell, *Nat. Mater.* **2004**, *3*, 302; e) J. Jin, Y. Wakayama, X. Peng, I. Ichinose, *Nat. Mater.* **2007**, *6*, 686; f) Z. Niu, J. Du, X. Cao, Y. Sun, W. Zhou, H. H. Hng, J. Ma, X. Chen, S. Xie, *Small* **2012**, *8*, 3201; g) H. Bai, C. Li, G. Shi, *Adv. Mater.* **2011**, *23*, 1089.

[16] T. Nishikawa, R. Ookura, J. Nishida, K. Arai, J. Hayashi, N. Kurono, T. Sawadaishi, M. Hara, M. Shimomura, *Langmuir* **2002**, *18*, 5734.

[17] U. H. F. Bunz, *Adv. Mater.* **2006**, *18*, 973.

[18] E. Banin, A. Lozinski, K. M. Brady, E. Berenshtein, P. W. Butterfield, M. Moshe, M. Chevion, E. P. Greenberg, E. Banin, *Proc. Natl. Acad. Sci. USA* **2008**, *105*, 16761.

[19] W. Hu, C. Peng, W. Luo, M. Lv, X. Li, D. Li, Q. Huang, C. Fan, *ACS Nano* **2010**, *4*, 4317.

[20] H. Chen, M. B. Müller, K. J. Gilmore, G. G. Wallace, D. Li, *Adv. Mater.* **2008**, *20*, 3557.

[21] M. Ramstedt, N. Cheng, O. Azzaroni, D. Mossialos, H. J. Mathieu, W. T. S. Huck, *Langmuir* **2007**, *23*, 3314.

[22] A. Kumar, P. K. Vemula, P. M. Ajayan, G. John, *Nat. Mater.* **2008**, *7*, 236.

[23] B. C. Allison, B. M. Applegate, J. P. Youngblood, *Biomacromolecules* **2007**, *8*, 2995.

[24] M. L. Schipper, N. Nakayama-Ratchford, C. R. Davis, N. W. S. Kam, P. Chu, Z. Liu, X. Sun, H. Dai, S. S. Gambhir, *Nat. Nanotechnol.* **2008**, *3*, 216.

[25] T. M. Benn, P. Westerhoff, *Environ. Sci. Technol.* **2008**, *42*, 4133.

[26] a) Y. Cui, L. Liu, B. Li, X. Zhou, N. Xu, *J. Phys. Chem. C* **2010**, *114*, 2434; b) J. Liu, H. Bai, Y. Wang, Z. Liu, X. Zhang, D. D. Sun, *Adv. Funct. Mater.* **2010**, *20*, 4175.

[27] F.-T. Kong, S.-Y. Dai, K.-J. Wang, *Adv. Optoelectron.* **2007**, 75384.

[28] a) J. R. Jennings, A. Ghicov, L. M. Peter, P. Schmuki, A. B. Walker, *J. Am. Chem. Soc.* **2008**, *130*, 13364; b) D. Kuang, J. r. m. Brillet, P. Chen, M. Takata, S. Uchida, H. Miura, K. Sumioka, S. M. Zakeeruddin, M. Grätzel, *ACS Nano* **2008**, *2*, 1113.

[29] A. Kongkanand, R. Martínez Domínguez, P. V. Kamat, *Nano Lett.* **2007**, *7*, 676.

[30] D. Wang, H. Duan, H. Mohwald, *Soft Matter* **2005**, *1*, 412.

[31] a) S. Stankovich, D. A. Dikin, R. D. Piner, K. A. Kohlhaas, A. Kleinhammes, Y. Jia, Y. Wu, S. T. Nguyen, R. S. Ruoff, *Carbon* **2007**, *45*, 1558; b) G. Zeng, Y. Xing, J. Gao, Z. Wang, X. Zhang, *Langmuir* **2010**, *26*, 15022.

[32] H.-F. Wang, L.-Y. Chen, W.-N. Su, J.-C. Chung, B.-J. Hwang, *J. Phys. Chem. C* **2010**, *114*, 3185.

[33] a) K. S. Kim, Y. Zhao, H. Jang, S. Y. Lee, J. M. Kim, K. S. Kim, J.-H. Ahn, P. Kim, J.-Y. Choi, B. H. Hong, *Nature* **2009**, *457*, 706; b) H. Park, P. R. Brown, V. Bulovi , J. Kong, *Nano Lett.* **2012**, *12*, 133.

[34] a) W. S. Hummers, R. E. Offeman, *J. Am. Chem. Soc.* **1958**, *80*, 1339; b) S. Park, R. S. Ruoff, *Nat. Nanotechnol.* **2009**, *4*, 217.